Structural and Functional Role of the Extracellular S5-P Linker in the HERG Potassium Channel

Jie Liu, Mei Zhang, Min Jiang, and Gea-Ny Tseng

Department of Physiology, Virginia Commonwealth University, Richmond, VA 23298

ABSTRACT C-type inactivation in the HERG channel is unique among voltage-gated K channels in having extremely fast kinetics and strong voltage sensitivity. This suggests that HERG may have a unique outer mouth structure (where conformational changes underlie C-type inactivation), and/or a unique communication between the outer mouth and the voltage sensor. We use cysteine-scanning mutagenesis and thiol-modifying reagents to probe the structural and functional role of the S5-P (residues 571–613) and P-S6 (residues 631–638) linkers of HERG that line the outer vestibule of the channel. Disulfide formation involving introduced cysteine side chains or modification of side chain properties at "high-impact" positions produces a common mutant phenotype: disruption of C-type inactivation, reduction of K^+ selectivity, and hyperpolarizing shift in the voltage-dependence of activation. In particular, we identify 15 consecutive positions in the middle of the S5-P linker (583–597) where side chain modification has marked impact on channel function. Analysis of the degrees of mutation-induced perturbation in channel function along 583–597 reveals an α-helical periodicity. Furthermore, the effects of MTS modification suggest that the NH_2-terminal of this segment (position 584) may be very close to the pore entrance. We propose a structural model for the outer vestibule of the HERG channel, in which the 583–597 segment forms an α-helix. With the NH_2 terminus of this helix sitting at the edge of the pore entrance, the length of the helix (~20 Å) allows its other end to reach and interact with the voltage-sensing domain. Therefore, the "583–597 helix" in the S5-P linker of the HERG channel serves as a bridge of communication between the outer mouth and the voltage sensor, that may make important contribution to the unique C-type inactivation phenotype.

KEY WORDS: rapid delayed rectifier K channel • LQT2 • cysteine-scanning mutagenesis • oocyte expression

INTRODUCTION

Human ether-a-go-go–related gene (*HERG*)* encodes the pore-forming subunit of the rapid delayed rectifier potassium (I_{Kr}) channel (Sanguinetti et al., 1995), an important determinant of action potential (AP) configuration and duration in human heart (Tseng, 2001). Suppression of I_{Kr} function due to inherited mutations in *HERG,* or more importantly due to adverse drug effects, has been linked to congenital or acquired long QT syndrome (Splawski et al., 2000), indicating an important role of HERG/I_{Kr} in maintaining the electrical stability of the heart. Under physiological conditions, the HERG/I_{Kr} channel passes little outward current at depolarized voltages (e.g., during phase 2 of cardiac AP) (Hancox et al., 1998; Zhou et al., 1998). This helps reduce the amount of inward current needed to maintain the plateau phase. Upon membrane repolarization (phase 3 of cardiac AP), there is a resurgence of outward current through the HERG/I_{Kr} channel that ensures proper return of voltage to the resting membrane potential (Hancox et al., 1998; Zhou et al., 1998). Such a "rectification" property of HERG/I_{Kr} is due to a fast inactivation process that can be turned on (by membrane depolarization) or off (by repolarization) in a matter of milliseconds (Spector et al., 1996).

The fast inactivation process of HERG/I_{Kr} shares important features with those of "C-type inactivation" in the Shaker channel (Hoshi et al., 1991; Yellen et al., 1994; Smith et al., 1996). These include the sensitivity to mutations introduced to the outer mouth region of the channel, slowing of the inactivation process by an outer mouth blocker (e.g., TEA), or by an increase in pore occupancy by permeant ions (e.g., K^+) (Hoshi et al., 1991; Yellen et al., 1994; Smith et al., 1996). Shaker's C-type inactivation has been well studied. It is due to conformational changes around the outer mouth, that constrict the pore or change the pore's selectivity in such a way that K^+ flux is prevented (Yellen et al., 1994; Liu et al., 1996; Starkus et al., 1997). The C-type inactivation process in the Shaker channel and in other voltage-gated K (Kv) channels for which C-type inactivation has been described (Kv1.3 [Panyi et al., 1995], Kv1.4 [Rasmusson et al., 1995], Kv1.5 [Fedida et al., 1999], and Kv2.1 [Klemic et al., 1998]) share two common features: slow kinetics and a lack of intrinsic voltage dependence. The slow kinetics is at least par-

Address correspondence to Gea-Ny Tseng, Department of Physiology, Virginia Commonwealth University, 1101 E. Marshall Street, Richmond, VA 23298. Fax: (804) 828-7382; E-mail: gtseng@hsc.vcu.edu

Abbreviations used in this paper: AP, action potential; HERG, human ether-a-go-go–related gene; MTS, methanethiosulfonate; WT, wild-type.

J. Gen. Physiol. © The Rockefeller University Press • 0022-1295/2002/11/723/15 $5.00
Volume 120 November 2002 723–737
http://www.jgp.org/cgi/doi/10.1085/jgp.20028687

tially attributed to hydrogen bonds formed around the outer mouth of the pore (Doyle et al., 1998; Larsson and Elinder, 2000; Ortega-Saenz et al., 2000). These hydrogen bonds stabilize the outer mouth in the open state, resisting collapse during C-type inactivation (Larsson and Elinder, 2000; Ortega-Saenz et al., 2000). The trigger for C-type inactivation in Shaker and related Kv channels is believed to be the S4 movements induced by membrane depolarization (Gandhi et al., 2000). Therefore, C-type inactivation in these channels is not intrinsically voltage sensitive, but derives its voltage sensitivity from a coupling to the voltage-dependent activation process. C-type inactivation in the HERG channel is extremely fast, and is intrinsically voltage-sensitive: it can occur at a time scale and in a voltage range with little or no channel activation (Sanguinetti et al., 1995; Rasmusson et al., 1998). What is the structural basis for these unique features of C-type inactivation in the HERG channel?

Fig. 1 shows an alignment of amino acid sequences that line the outer vestibule (S5-P and P-S6 linkers) and the outer portion of the pore (pore or P-loop) of HERG, KcsA (the bacterial proton-gated K channel whose crystal structure has been solved [Doyle et al., 1998]), and major classes of Kv channel. This comparison reveals two unique features of the HERG sequence. First, amino acids that are implicated in forming hydrogen bonds that stabilize the Shaker outer mouth in the open state (E418, W434, and Y445, highlighted by gray shade in Fig. 1) are well conserved among Kv channels as well as in KcsA, but are missing in HERG. This reduced hydrogen bonding capability in HERG may make its outer mouth more flexible, easier to collapse by conformational changes triggered by membrane depolarization. This can contribute to the uniquely fast C-type inactivation kinetics in the HERG channel. Second, the S5-P linker in the HERG channel is much longer than those of KcsA and other Kv channels (43 aa vs. 14–23 aa). This long S5-P linker may play a unique role in the structure and function of the HERG channel.

Previously, we have shown that replacing the histidine at position 587 in the middle of HERG's S5-P linker (circled in the HERG sequence in Fig. 1) to proline or cysteine in disulfide-bonded state has profound effects on three aspects of channel function: (a) disrupting C-type inactivation, (b) reducing K^+ selectivity, (c) accelerating activation, and causing a hyperpolariz-

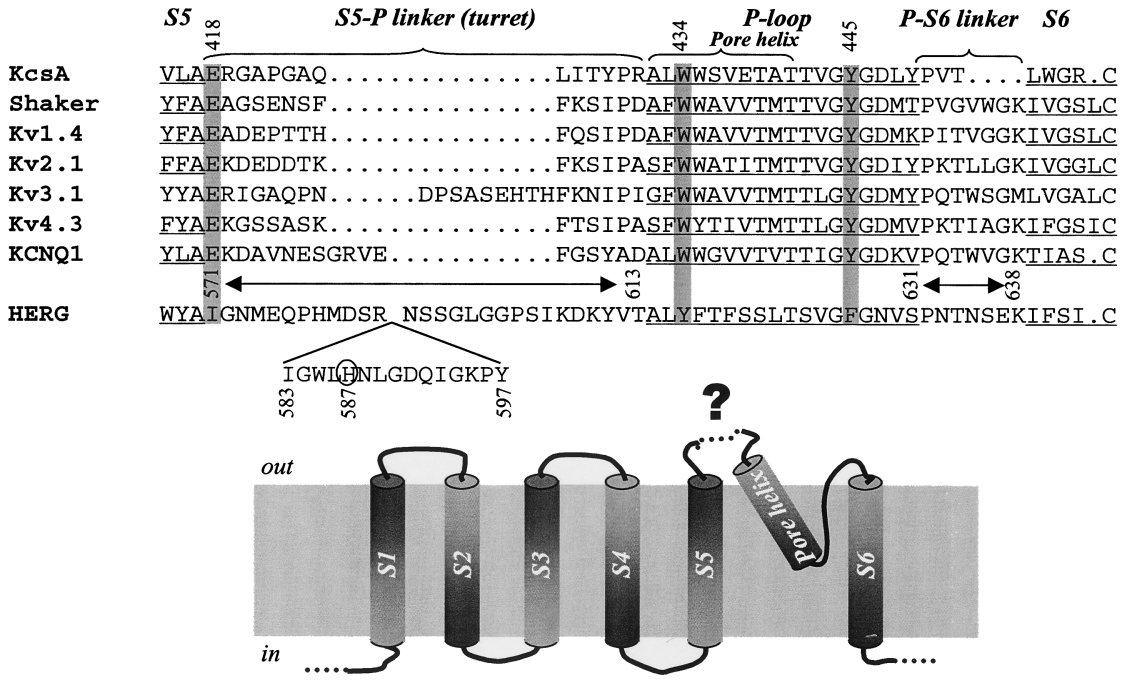

FIGURE 1. (Top) Alignment of amino acid sequences from the end of S5 to the beginning of S6 of HERG, major classes of voltage-gated K (Kv) channels, and KcsA. Transmembrane and pore (P)-loop regions are underlined. S5 and S6 correspond to M1 and M2 of KcsA, respectively. S5-P linker ("turret" of KcsA) and P-S6 linker (P-M2 of KcsA) are marked. Gaps (...) are introduced to improve alignment. Amino acids in the Shaker channel implicated in hydrogen bonding and critical for maintaining the outer mouth in the open state are highlighted by gray shade: E418, W434, and Y445 (Shaker position numbers shown on top). Note that these amino acids are conserved in KcsA and all major classes of Kv channels, but not in HERG. The HERG positions examined here (571–613 of S5-P linker, and 631–638 of P-S6 linker) are marked above its sequence. Positions 583–597 are shown as an insert. H587 in HERG is circled (see text for discussion). (Bottom) Transmembrane topology of one Kv channel subunit. The structure of the unusually long extracellular S5-P linker of HERG (marked by a dotted line and "?") is the major focus of this study.

ing shift in the voltage dependence of activation (Dun et al., 1999a). On the other hand, substituting H587 with cysteine in reduced state has little or no impact on the above channel function (Dun et al., 1999a). Since position 587 is far from the P-loop in a one-dimensional sequence, how do mutations here affect the outer mouth properties (C-type inactivation and K^+ selectivity)? How is this position involved in the activation gating process? We hypothesized that the long S5-P linker of the HERG channel does not assume a random coil conformation, as is the case for the much shorter "turret" (the S5-P equivalent) in the KcsA crystal structure (Doyle et al., 1998). Instead, this linker may assume certain secondary structure around position 587 and make contacts with other domains of the channel. Therefore, perturbing the conformation here by replacing H587 with proline or by disulfide formation in H587C can affect several aspects of channel function.

To explore the role of the S5-P linker in HERG channel function, and to test whether there is a secondary structure in this extracellular domain, we apply cysteine-scanning mutagenesis to positions 571–613 of HERG. We also include the P-S6 linker (positions 631–638) because, as suggested by the crystal structure of KcsA and by functional studies on the Shaker channel, it interacts with the S5-P linker during gating processes (Doyle et al., 1998; Gandhi et al., 2000; Larsson and Elinder, 2000; Ortega-Saenz et al., 2000). The wild-type (WT) HERG channel has 12 native cysteines that are functionally "silent": channel function is not affected by treatment with DTT, H_2O_2, or extracellular MTS reagents (Dun et al., 1999a; Fan et al., 1999). Therefore, cysteine substitutions are made in the WT HERG background. We examine: (a) channel behavior before and after DTT treatment, and (b) effects of extracellular MTSET or MTSES modification of introduced cysteine side chains on channel function. Based on these data, we propose a structural model for the outer vestibule of the HERG channel, in which the middle part of the S5-P linker assumes an α-helical structure and serves as a bridge of communication between the outer mouth and the voltage-sensing domain. Therefore, the S-P linker in HERG plays a central role in determining the voltage-sensitivity of the C-type inactivation process.

MATERIALS AND METHODS

Mutagenesis

HERG in a vector, pGH19 (a gift from Dr. Gail A. Robertson, University of Wisconsin-Madison, Madison, WI), was subcloned into the KpnI/XbaI site of a vector, pAlterMax, and subjected to cysteine scanning mutagenesis using the oligonucleotide-directed method (Altered site II in vitro mutagenesis system; Promega). Mutations were confirmed by direct DNA sequencing around the mutation sites. In most cases, two independent colonies were picked and used for cRNA transcription and oocyte expression. No differences in the channel phenotype were noticed between two colonies from the same mutant. For transcription, plasmids were linearized by NotI and transcribed using T7 RNA polymerase using a commercial kit (Mmessage Mmachine; Ambion). The quality and quantity of cRNA products were evaluated using densitometry (ChemiImager model 4400; α-Innotech Corp.).

Oocyte Preparation

Oocytes from *Xenopus laevis* were isolated as described before (Tseng-Crank et al., 1990), and incubated in an ND96-based medium (in mM: NaCl 96, KCl 2, $CaCl_2$ 1.8, $MgCl_2$ 1, HEPES 5, Na-pyruvate 2.5, pH 7.5, supplemented with 4% horse serum and penicillin/streptomycin) at 16°C. Five to 12 h after isolation, each oocyte was injected with 40 nl of cRNA solution (containing 4–18 ng cRNA), using a Drummond digital microdispenser. Oocytes were incubated in the above medium at 16°C, and studied 2–4 d after cRNA injection.

Voltage Clamp Experiments

Membrane currents were recorded from whole oocytes using the "2-cushion pipette" voltage clamp method (Schreibmayer et al., 1994). Both the current-passing and voltage-recording pipettes were filled with 3 M KCl and the tips were plugged with 1% agar in 3 M KCl (tip resistance 0.1–0.3 MΩ). During recordings, the oocyte was continuously superfused with a low Cl ND96 solution to reduce interference from endogenous Cl channels (in mM: NaOH 96, KOH 2, $CaCl_2$ 1.8, $MgSO_4$ 1, HEPES 5, Na-pyruvate 2.5, titrated to pH 7.5 with methanesulfonic acid). The grounding electrodes (containing Ag/AgCl pellets) are filled with 3 M KCl and connected to the bath solution via salt bridges made of 1% agar in 3 M KCl. In some experiments on cysteine-substituted mutants that were poorly expressed, $[K^+]_o$ was elevated from 2 to 98 mM ($[Na^+]_o$ removed to maintain the osmolality) to increase current amplitude and facilitate current measurements. This will be specified in the text or figure legends. Voltage clamp was done at room temperature (24–26°C) with OC-725B or OC-725C amplifier (Warner Instruments). Voltage clamp protocol generation and data acquisition were controlled by pClamp5.5 via a 12-bit D/A and A/D converter (DMA; Axon Instruments, Inc.). Current data were low-pass filtered at 1 kHz (Frequency Devices) and stored on disks for off-line analysis.

Data Analysis

Most of the voltage clamp protocols and methods of data analysis are described in the text or figure legends. The following software was used for data analysis: pClamp6 or 8, EXCEL (Microsoft), SigmaPlot, SigmaStat, and PeakFit (SPSS).

To explore α-helical periodicity in mutation-induced perturbations of channel function, we used a Fourier transform method as described (Cornette et al., 1987; Li-Smerin et al., 2000). Assuming that channels are distributed between only two states, closed and open, the free energy needed (ΔG_o) when channels are moved from closed to open states at 0 mV is:

$$\Delta G_0 = RT(V_{0.5}/k), \quad (1)$$

where R is the universal gas constant and T is absolute temperature. $V_{0.5}$ is the half-maximum activation voltage and k is the slope factor obtained from fitting the activation curve with a Boltzmann function (Fig. 5 legend, see equation). In cases when a double Boltzmann function is required to fit the activation curve, $V_{0.5}$ and k are the parameter values from the Boltzmann compo-

nent in the more negative voltage range (see Fig. 6). Mutation-induced perturbation in ΔG_o is calculated as:

$$\Delta\Delta G_0 = \Delta G_0^{MUT} - \Delta G_0^{WT}, \quad (2)$$

where ΔG_o^{MUT} and ΔG_o^{WT} are ΔG_o values for mutant and WT HERG channels, respectively. A Fourier transform method was used to evaluate the periodicity of $\Delta\Delta G_o$, according to:

$$P(\omega) = [X(\omega)]^2 + [Y(\omega)]^2,$$

$$\text{where } X(\omega) = \sum_{j=0}^{n-1} [(Vj - \langle V\rangle)\sin(j\omega)] \text{ and}$$

$$Y(\omega) = \sum_{j=0}^{n-1} [(Vj - \langle V\rangle)\cos(j\omega)]$$

$P(\omega)$ is the Fourier transform power spectrum as a function of angular frequency (ω), "n" is the number of residues within the segment under analysis, Vj is $|\Delta\Delta G_o|$ at a given position "j + 1" in the segment, and <V> is the average value of $|\Delta\Delta G_o|$ of the segment. To evaluate the α-helical characteristics of a power spectrum, an α-periodicity index (α-PI) is calculated as:

$$\alpha\text{-PI} = [1/30\int_{90°}^{120°} P(\omega)d\omega]/[1/180\int_{0°}^{180°} P(\omega)d\omega]. \quad (3)$$

Cysteine Side Chain Modifications

DTT stock solution (0.5 M in deionized water) was frozen at −20°C in small aliquots. An aliquot was thawed and diluted to 5 mM in bath solution immediately before use. MTSET or MTSES powder (Toronto Research Chemicals) was dissolved in deionized water at 0.1 M shortly before experiments. The stock solution was stored on ice and used within 2 h. After control data were obtained, the MTSET or MTSES stock solution was diluted with bath solution to 1 mM and applied immediately to the oocyte. After treatment with DTT, MTSET, or MTSES, effects on the function of cysteine-substituted channels were evaluated after a 10–15 min washout period to ascertain that the effects resulted from covalent modifications.

RESULTS

Of the 51 cysteine-substituted HERG mutants we made, three (N573C, K595C and K638C) do not produce functional channels and are not included in the experiments reported here. For the remaining 48 mutants, we characterize their channel phenotypes before and after DTT treatment by measuring three parameters of channel function: (a) degree of C-type inactivation, (b) selectivity for K^+ over Na^+ ions, and (c) voltage dependence of activation. We also examine the effects of two thiol-modifying methanethiosulfonate (MTS) reagents, MTSET and MTSES, on these cysteine-substituted mutants. Modifications of thiol side chains by both MTS reagents increase the side chain volume, but MTSET adds a positive charge while MTSES adds a negative charge. A comparison of their effects on channel function may provide clues as to the location or environment of the thiol side chains. For example, modification of a side chain inside a narrow pore or crevice by both MTS reagents may cause a similar effect due to steric hindrance of ion permeation or protein conformational changes. On the other hand, modification of a side chain on the channel surface close to the pore entrance or to the voltage sensor by the two MTS reagents likely will lead to different or opposite changes, due to electrostatic effects on the local ion concentrations around the pore or on the local electrical field sensed by the voltage sensor.

In the following sections, we will first use data from two mutants (I583C and W585C), along with data from the WT HERG, to illustrate the voltage clamp protocols and data analysis used to characterize the channel phenotypes. We then summarize data from all 48 cysteine mutants. The data allow us to deduce positions in the S5-P and P-S6 linkers where side chain properties are critical for the HERG channel function. Finally, we will focus on two specific issues: (a) periodicity of mutation-induced perturbations of channel function, and (b) effects of MTS modification of pore-entrance residues. These data reveal better defined features in the outer vestibule structure of the HERG channel.

Characterizing I583C and W585C and Comparing them with WT HERG

C-type inactivation and K^+ selectivity before and after DTT treatment. In Fig. 2, data for each of the three channels (WT HERG, I583C, and W585C) are taken from the same oocyte before and after DTT treatment, a reducing agent whose only action is to break disulfide bonds. The voltage clamp protocol is diagrammed on top of column B: from a holding voltage (V_h) of −80 mV, prepulses to 60 mV for 0.2 s are used to fully activate the channels and, if the C-type inactivation is present, to cause channel inactivation. These prepulses are followed by repolarizing steps to V_r ranging from 30 to −120 mV. During the repolarizing steps, channels rapidly (τ of a few ms) reach new, lower levels of C-type inactivation determined by V_r. At V_r −40 mV or more negative, recovery from C-type inactivation is followed by deactivation. The tail current (I_{tail}) amplitudes are measured from the plateau level (at V_r positive to −40 mV) or the peak level (at V_r −40 mV or more negative). To pool data from different cells, I_{tail} amplitudes of each cell are normalized by the maximal outward tail current from the same cell. For WT HERG and WT-like mutants (e.g., I583C after DTT treatment, see below), the maximal outward currents occur at V_r −60 mV. For mutants with altered behavior (e.g., I583C before DTT), the maximal outward tail currents are taken from those at V_r 30 mV.

The amplitudes of these tail currents are determined by two factors: (a) steady-state level of C-type inactivation at V_r, and (b) driving force for currents through the channels (difference between V_r and the reversal potential, E_{rev}). For WT HERG (Fig. 2 A), there is little

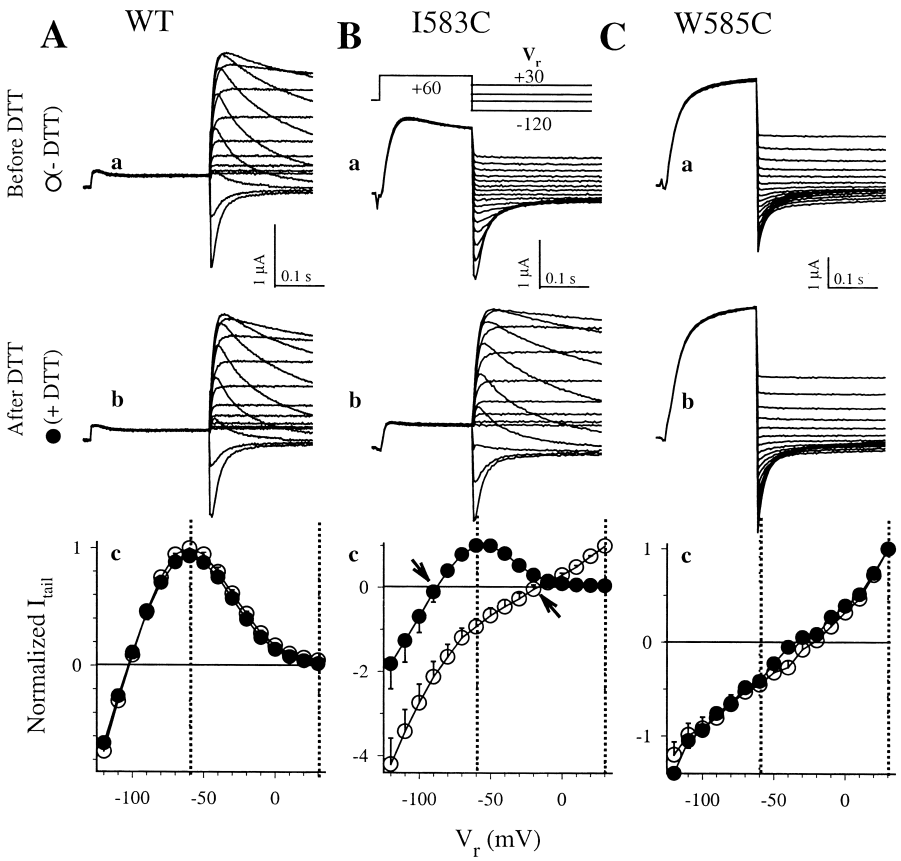

FIGURE 2. Effects of cysteine substitution at positions 583 and 585 on the I-V relationship and reversal potential (E_{rev}) of HERG. These experiments are done in 2 mM $[K]_o$ and 96 mM $[Na]_o$, using the voltage clamp protocol shown on top of B. Original current traces recorded from WT HERG (A), I583C (B) and W585C (C) before DTT treatment (a), and after DTT treatment (b; 5 mM DTT for 10–15 min, followed by ~10-min wash) from the same oocytes are shown. Tail current amplitudes are measured, leak-subtracted, and normalized by the maximal outward tail currents measured from the same oocytes. Average I-V relationships are summarized in panels c. Dotted lines denote the V_r range (30 to −60 mV) where the slopes of the I-V relationships are used for the calculation of "rectification factors" (Fig. 6). Arrows in panel c of B point to E_{rev} of I583C before and after DTT treatment.

outward current at 60 mV or at $V_r > 0$ mV due to a strong C-type inactivation process. As V_r goes from 0 to −60 mV, I_{tail} becomes more outward due to a voltage-dependent recovery from C-type inactivation. At more negative V_r, the tail current decreases in amplitude because the decrease in driving force outweighs the decrease in the level of C-type inactivation. Therefore, outward I_{tail} peaks at −60 mV and the tail I-V relationship has a negative slope in the V_r range of 30 to −60 mV. The tail current reverses at an E_{rev} of −100 mV. Based on the constant field equation (Fig. 6 legend), the E_{rev} corresponds to a high permeability ratio of K^+ to Na^+ (P_K/P_{Na} = 481 ± 129, n = 8). DTT treatment does not induce any significant changes in the kinetics or tail I-V relationship of WT HERG, confirming that the native cysteine side chains in the HERG channel do not engage in disulfide formation.

I583C before DTT treatment has a very different tail I-V relationship from that of WT HERG (Fig. 2 B, a). There is a prominent outward current at 60 mV. Repolarizing steps elicit smaller outward tail currents that reverse at about −20 mV. Therefore, there is a positive slope in the tail I-V relationship in the V_r range of 30 and −60 mV (panel c, open circles). This reflects the change in driving force for current through the channels. Therefore, the C-type inactivation process is disrupted in I583C under these conditions. Furthermore, the E_{rev} (−21.1 ± 6.9 mV) is much more positive than that of WT HERG. Removing extracellular Na^+ ions shifts the E_{rev} in the negative direction toward E_K, indicating that Na^+ ions can permeate through the I583C channels under these conditions. The calculated P_K/P_{Na} is 2.3 ± 1.0 (n = 6).

Fig. 2 B, b and c (closed circles), shows that DTT treatment converts the I583C channel phenotype from the mutant behavior to a "WT-like" behavior. DTT-treated I583C shows a prominent negative slope in the tail I-V relationship, indicating a restoration of the C-type inactivation process. DTT treatment also causes a negative shift in E_{rev} (to −93.4 ± 2.6 mV), indicating an increase in P_K/P_{Na} (to 117.6 ± 32.4). These observations indicate that the introduced cysteine side chains in I583C are disulfide bonded before DTT treatment. Under these conditions, the channel function (C-type inactivation and K^+ selectivity) is disrupted. However, when the cysteine side chains are reduced to the free thiol state, channel function is well maintained.

W585C manifests a mutant behavior similar to that of I583C before DTT treatment: a positive slope in the tail I-V relationship in the V_r range of 30 to −60 mV and an E_{rev} of −23.3 ± 5.5 mV (P_K/P_{Na} = 2.1 ± 0.5, n = 5) (Fig. 2 C, a and c). However, unlike I583C, DTT treatment did not convert the mutant behavior to a WT-like behavior (although the W585C current amplitude is

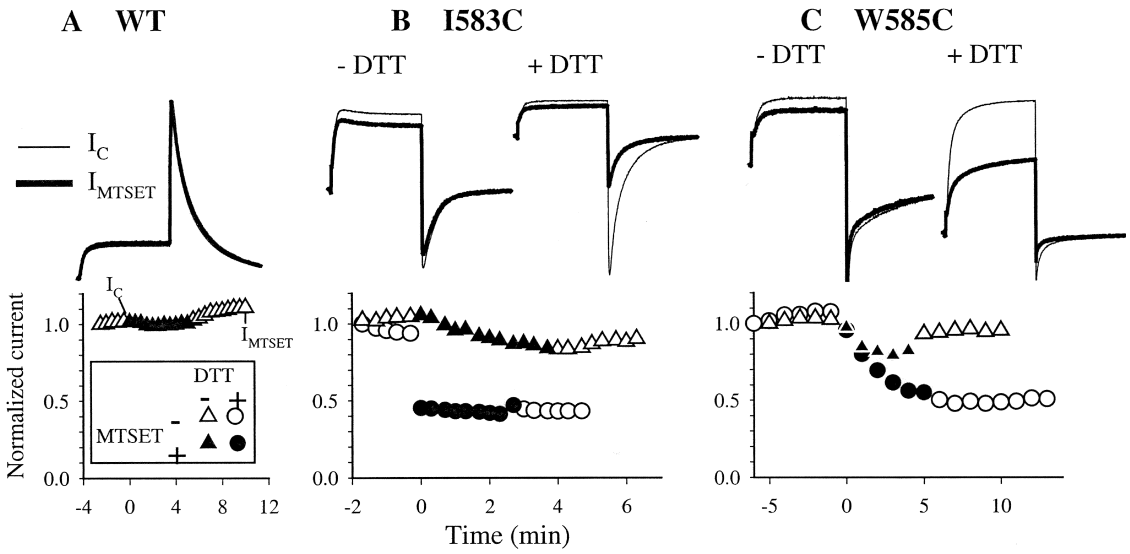

FIGURE 3. MTSET has no effects on WT HERG (A), and its effects on I583C (B) and W585C (C) are enhanced by DTT pretreatment. In each panel, the upper part illustrates superimposed current traces under the control conditions (I_C, thin trace) and after MTSET treatment (I_{MTSET}, thick trace). I_C is measured right before MTSET exposure, and I_{MTSET} is measured after MTSET washout. An example of the time points at which I_C and I_{MTSET} are sampled is denoted in the time course of A. WT HERG has no DTT-treatment. I583C and W585C are either not DTT-treated (−DTT), or DTT-pretreated (+DTT, 5 mM for up to 4 h). −DTT and +DTT data are from different cells. The lower parts show time courses of changes in the peak amplitude of tail current before, during and after MTSET exposure from the same experiments as shown in the upper parts. Time zero marks the beginning of MTSET (1 mM) superfusion. Open symbols are data points recorded before and after MTSET exposure, whereas closed symbols are those during MTSET exposure. Triangles denote data from cells without DTT treatment, and circles are data from cells pretreated with DTT. (A) WT HERG recorded in 2 mM $[K]_o$, channel is activated by 1-s depolarization pulses to 20 mV, and tail currents are recorded at −80 mV. (B) I583C recorded in 2 mM $[K]_o$, activated by 1-s depolarization to 60 mV, tail currents recorded at −80 mV. (C) W585C recorded in 98 mM $[K]_o$, activated by 1-s depolarization to 20 mV, tail currents recorded at −120 mV.

modestly increased by DTT treatment; see also of Fig. 5 C, a and b). Relatively aggressive DTT treatment (5 mM for 4 h) cannot convert the W585C phenotype to the WT-like behavior. There are two possible explanations for this apparent resistance of W585C's mutant phenotype to DTT treatment. First, the introduced cysteine side chains in W585C form very stable disulfide bonds that cannot be reduced under our experimental conditions. Second, the tryptophan side chain at 585 is critical for channel function so that replacing it with cysteine, even in the reduced free thiol state, disrupts the C-type inactivation and K^+ selectivity.

Effects of MTSET and MTSES before and after DTT treatment. To distinguish between these two possibilities, we test the effects of MTS reagents (MTSET and MTSES) on W585C before and after DTT treatment. MTS reagents can modify free thiol side chains, but not thiol side chains engaged in stable disulfide bonds. Therefore, if DTT-treated W585C has free thiol groups despite the mutant behavior, extracellular MTS should be able to modify the side chains and alter channel function. Furthermore, if there is disulfide formation in W585C before DTT treatment, the MTS effects should be enhanced by DTT treatment.

Figs. 3 A and 4 A show that MTSET or MTSES treatment has no effects on WT HERG. These confirm that native cysteines in HERG are not accessible, or not reactive, to extracellular MTS reagents. Therefore, we are confident that the effects of MTS treatment on cysteine-substituted mutants are due to modification of the introduced cysteine side chains. Fig. 3 B shows that the effect of MTSET on I583C is enhanced by DTT treatment. This is consistent with the notion that the introduced cysteine side chains in I583C are disulfide bonded before DTT treatment. This causes a disruption of channel function (C-type inactivation and K^+ selectivity) and a low MTSET sensitivity. Breaking the disulfide bonds by DTT restores the channel function and increases MTSET sensitivity.

Fig. 3 C shows that before DTT treatment MTSET has a very small suppressing effect on W585C. DTT treatment markedly enhances MTSET effect on W585C. These data confirm the second possibility listed above: the introduced cysteine side chains in W585C can form disulfides. DTT breaks the disulfides and enhances MTSET sensitivity, but does not restore the WT-like behavior. Therefore, the tryptophan residue at 585 is critical for HERG channel function. In addition, the increase in W585C current amplitude after DTT treatment indicates that disulfide formation in W585C suppresses current amplitude.

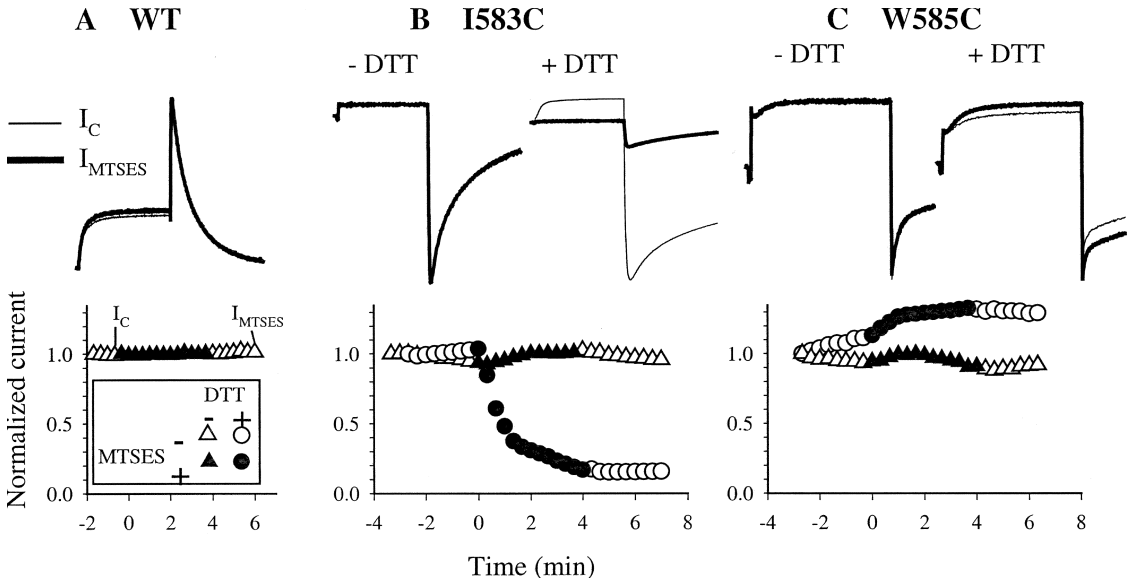

FIGURE 4. Effects of MTSES on WT HERG (A), I583C (B) and W585C (C). The format of this figure is the same as that in Fig. 3. (A) WT HERG recorded in 2 mM $[K]_o$, activated by 1-s depolarization pulses to 20 mV, tail currents recorded at −80 mV. (B) I583C recorded in 98 mM $[K]_o$, activated by 1-s depolarization to 20 mV, tail currents recorded at −80 mV. (C) W585C recorded in 98 mM $[K]_o$, activated by 1-s depolarization to 20 mV, tail currents recorded at −120 mV.

Fig. 4, B and C, illustrate the effects of MTSES on I583C and W585C before and after DTT treatment. Consistent with data shown in Fig. 3, without DTT treatment MTSES has little effects on either channels. After DTT treatment, MTSES markedly suppresses the I583C current amplitude but modestly increases the W585C current amplitude. Therefore, MTSET and MTSES have qualitatively the same effect on I583C, but different effects on W585C. The implication of these observations will be addressed in the context of the proposed structural model for HERG's outer vestibule (see DISCUSSION).

Voltage-dependence of activation before and after DTT treatment. Fig. 5 illustrates the voltage clamp protocol and data analysis used to characterize the voltage dependence of activation of WT HERG and the two mutant channels. The protocol is diagrammed in the middle of column A. From V_h −80 mV, 1-s test pulses to V_t from −70 to 60 mV are applied at 10-mV increments. The peak amplitudes of tail currents are measured and normalized by the maximum tail current following V_t to 60 mV. This gives an estimate of the fraction of channels activated at the end of the previous test pulse to V_t. For WT HERG and WT-like mutants (e.g., I583C after DTT), the tail currents are measured at −80 mV at which the currents are outward and large (Fig. 5, A and B, b). For mutants with altered behavior (e.g., I583C before DTT), tail currents at −80 mV are inward and small due to changes in ion permeation properties. Therefore, a more hyperpolarized voltage (−120 mV) is used to increase the amplitude of inward tail currents and facilitate measurement.

WT HERG has the same voltage dependence of activation before and after DTT treatment (Fig. 5 A). The activation curve is well described by a single Boltzmann function, with an average half-maximum activation voltage ($V_{0.5}$) of −17.0 ± 1.5 mV (n = 14). On the other hand, without DTT treatment I583C manifests a more negative Boltzmann component ($V_{0.5}$ = −40.2 ± 0.9 mV, n = 6, Fig. 5 B, c, open circles) than that of WT HERG. Furthermore, there appears a slowly rising phase of channel activation in the positive voltage range. Therefore, the activation curve requires a second Boltzmann component for a good fit (Fig. 5 legend). DTT treatment of I583C restores the WT-like behavior: the activation curve now follows a single Boltzmann function. The $V_{0.5}$ value is similar to that of WT HERG (−13.4 ± 2.4 mV, n = 5, Fig. 5 B, c, closed circles). W585C manifests the mutant behavior before and after DTT treatment: its activation curves under both conditions require a double Boltzmann function for a good fit, and the $V_{0.5}$ values of the negative Boltzmann component are more negative than the $V_{0.5}$ of WT HERG (−31.5 ± 3.7 mV, n = 5, and −27.4 ± 3.0 mV, n = 7, before and after DTT, respectively).

Summary of Effects of Cysteine Substitutions in the S5-P and P-S6 Linkers on HERG Channel Function, and Effects of MTSET or MTSES Modification

We apply the above voltage clamp protocols and data analysis to the other 46 cysteine-substituted mutant channels made in the S5-P linker (positions 571–613) and in the P-S6 linker (positions 631–637). Results are

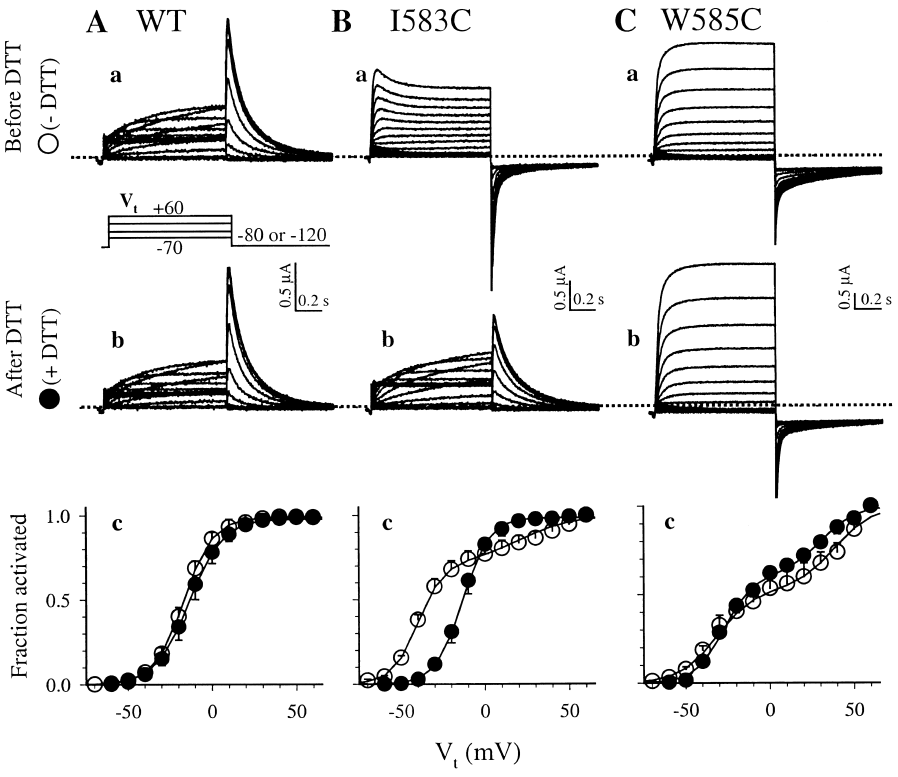

FIGURE 5. Effects of cysteine substitution at positions 583 and 585 on the voltage dependence of activation. The voltage clamp protocol is shown in the middle of column A. Superimposed original current traces recorded before DTT treatment (panels a), and after DTT treatment (panels b) from the same oocytes are depicted. Dotted lines denote the zero current level. Panels c illustrate 1-s isochronal activation curves averaged from 5–7 oocytes per group. For each oocyte, tail current amplitudes after depolarization to different levels of V_t are measured and normalized by the maximal tail current after V_t to 60 mV. This gives an estimate of the fraction of channels activated at the end of V_t. The relationship between V_t and "fraction activated" is fit with a single (WT, and I583C after DTT) or double (I583C before DTT, and W585C before/after DTT) Boltzmann function: Fraction activated = $A_1/\{1 + \exp[(V_1 - V_t)k_1]\} + A_2/\{1 + \exp[(V_2 - V_t)/k_2]\}$, where A_i, V_i, and k_i are the fraction, half-maximum activation voltage and slope factor of *i*th Boltzmann component. For single Boltzmann function, i = 1 only. The superimposed activation curves are calculated from appropriate Boltzmann function with mean parameter values.

summarized in Fig. 6. Fig. 6 A summarizes "rectification factors" (see equation in Fig. 6 legend), which indicate whether the C-type inactivation process is maintained (values < 0 or upward histogram bars) or interrupted (values > 0 or downward histogram bars). Fig. 6 B summarizes the permeability ratios of K^+ to Na^+ (P_K/P_{Na}). Fig. 6 C summarizes the half-maximum activation voltages ($V_{0.5}$) of the (major) Boltzmann component used to fit the activation curves (see equation, Fig. 5 legend). Fig. 6, D and E, summarize the ratios of currents after MTSET or MTSES treatment to control (I_{MTS}/I_C, as described in Figs. 3 and 4).

For WT HERG and mutants with WT-like behavior (prominent C-type inactivation and strong K^+ selectivity), the channel phenotypes are the same before and after DTT treatment. This indicates that the introduced cysteine side chains are mostly in the reduced state without DTT treatment. Therefore, data from both before and after DTT treatment are combined and shown as white histogram bars in Fig. 6. For mutant channels with altered behavior before DTT treatment, data obtained under these conditions are shown as open circles, while data obtained after DTT treatment are shown as gray histogram bars.

Based on Fig. 6, we can divide the degrees of impact on channel function of side chain modification into three groups: high-impact, intermediate-impact, and low-impact. High-impact positions are those where cysteine substitution disrupts the channel function even when the thiol groups are in the reduced state. This is revealed by a marked MTSET sensitivity with or without DTT treatment, despite the maintained mutant behavior. The three nonfunctional mutants (N573C, K595C, and K638C) are also included in this group. There are a total of 15 high-impact positions: three at the outer end of S5 (I571, G572, and N573), eight in the 583–597 segment (W585, L586, N588, L589, G590, D591, I593, and K595), one between the 583–597 segment and the P-loop (G604), and three in the P-S6 linker (P632, T634, and K638).

Intermediate-impact positions are those where cysteine substitution in free thiol state is well tolerated (WT-like behavior, some requiring DTT treatment due to disulfide formation), but further MTSET modification produces a significant impact on channel function. There are 10 intermediate-impact positions: seven in the 583–597 segment (I583, G584, H587, Q592, G594, P596, and Y597), one between the 583–597 segment and the P-loop (D609), and two at the two ends of the P-loop (T613 and S631).

There are 22 positions where introduced cysteine side chains are well tolerated (WT-like phenotype) and do not form disulfide bonds (DTT has no further effects). Importantly, MTSET treatment does not have

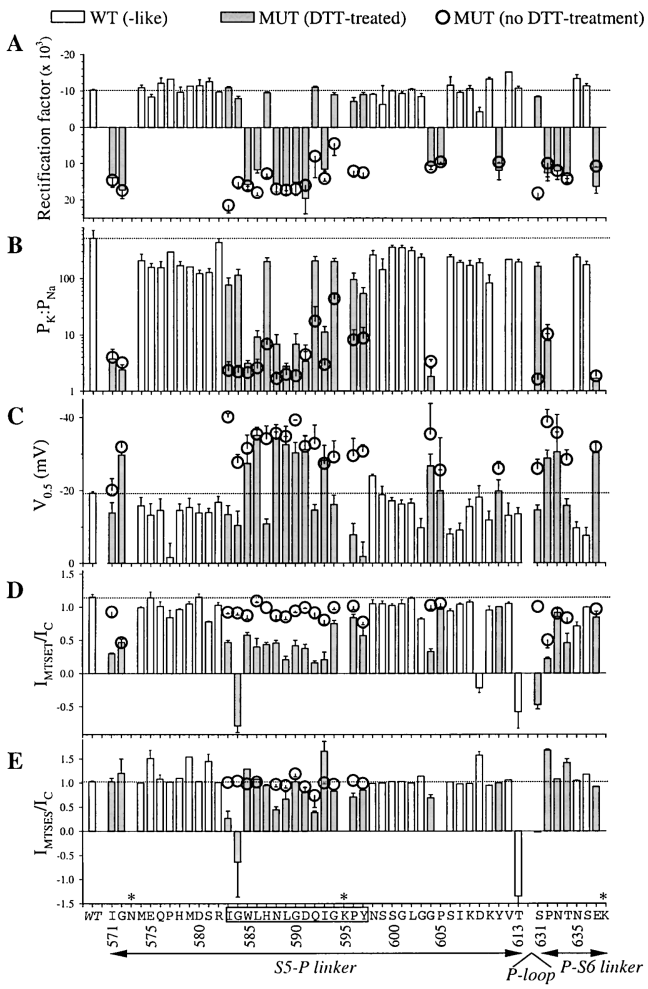

FIGURE 6. Summary of effects of cysteine substitutions in the S5-P and P-S6 linkers of HERG on the degree of C-type inactivation (A), K^+ ion selectivity (B), half-maximum activation voltage (C), response to MTSET (D), and response to MTSES (E). For all panels, white histogram bars denote data from WT HERG and WT-like mutants, gray histogram bars are data from mutants with altered behavior (MUT) after DTT treatment (5 mM, up to 4 h), and open circles are data from MUT without DTT treatment. Dotted lines are drawn across the WT data to facilitate comparison. Data are plotted against WT residues along the abscissa, with selected position numbers marked. The 583–597 segment is boxed. The channel domains (S5-P and P-S6 linkers, with P-loop in between) are also denoted. Asterisk indicates no expression (N573C, K595C, and K638C). (A) The degree of C-type inactivation is measured by a "rectification factor" calculated from the normalized tail I-V relationship as shown in Fig. 2: Rectification factor = $[(I_{+30} - I_{-60})/90]$, where I_{+30} and I_{-60} are the normalized tail currents at +30 and −60 mV, respectively. (B) K^+ ion selectivity is measured by the permeability ratio of K^+ to Na^+ (P_K/P_{Na}). This is calculated from the reversal potential (E_{rev}) measured in 2 mM $[K]_o$ and 96 mM $[Na]_o$ based on the constant field equation: $E_{rev} = RT\ln[(\alpha[K]_o + [Na]_o)/(\alpha[K]_i + [Na]_i)]$, where $\alpha = P_K/P_{Na}$, $[K]_i$ and $[Na]_i$ are assumed to be 125 and 10 mM, respectively, R is the gas constant, and T is the absolute temperature. P_K/P_{Na} is plotted on a logarithmic scale. Current amplitudes of P605C, Y611C, N633C, and T634C in 2 mM $[K]_o$ are too small for a reliable measurement of E_{rev}. (C) Half-maximum activation voltage ($V_{0.5}$) is obtained by fitting a Boltzmann function to 1-s isochronal activation curves as described for Fig. 5. When there are two Boltzmann components, the $V_{0.5}$ values reported here correspond to those of the negative (major) component. (D) Effects of MTSET are evaluated by ratio of I_{MTSET} to I_C. These current amplitudes are measured as shown in Fig. 3. (E) Effects of MTSES are evaluated in the same manner as described for MTSET, with I_C and I_{MTSES} measured as shown in Fig. 4. The negative values of I_{MTS}/I_C for G584C, D609C (MTSET but not MTSES), T613C, and S631C indicate a change in tail current direction at −80 mV from outward (I_C) to inward (I_{MTS}) (see Fig. 8).

significant irreversible effects on these cysteine-substituted channels. Since the WT residues at these positions are mostly hydrophilic or even charged, it is likely that the insensitivity to MTSET is not due to a lack of accessibility, but due to a lack of impact of side chain modification on channel function. Therefore, these are low-impact positions where side chains are most likely solvent (extracellular aqueous phase) exposed: 574–582, 598–603, 606–608, 610, 612, 635, and 636.

Finally, there are four positions (P605, Y611, N633, and E637) where cysteine substitution leads to a DTT-resistant mutant phenotype. These cysteine-substituted channels are insensitive to MTSET or MTSES even after aggressive DTT treatment. Therefore, it is unclear whether the introduced thiol side chains are in the reduced state but are not accessible or not reactive to extracellular MTSET or MTSES, or the introduced thiol side chains are in very stable disulfide bonds that cannot be broken by DTT under our experimental conditions. The low expression level of all four mutants suggests that the second possibility may be more likely.

A striking feature of these summary results is the shared common mutant phenotype. Therefore, perturbing the conformation of HERG's outer vestibule, either due to disulfide bond formation involving introduced cysteine side chains (as evidenced by a restoration of WT-like behavior after DTT treatment), or due to a replacement of residues at high-impact positions with cysteine (as evidenced by a prominent MTSET sensitivity after DTT-treatment despite the maintained mutant phenotype), leads to common results: a disruption of C-type inactivation (Fig. 6 A), a decrease in K^+ selectivity (Fig. 6 B), and a negative shift in $V_{0.5}$ of channel activation (Fig. 6 C). These observations support a key role played by HERG's outer vestibule in channel function. Note that the P_K/P_{Na} values are rough estimates of channel selectivity, because the intracellular K^+ and Na^+ concentrations are not directly measured. The estimated P_K/P_{Na} values may be mutant-dependent, because mutation-induced changes in membrane conductance may affect these intracellular ion concentrations. However, these uncertainties do not alter the conclusions listed above.

Another striking feature is the marked impact on channel function of cysteine substitution at 15 consecutive positions in the middle of the S5-P linker: the 583–597 segment (including 587 studied previously [Dun et

al., 1999a]). K595C destroys functional expression. The other 14 channels all manifest the common mutant phenotype before DTT treatment. After DTT, seven assume the WT-like behavior: I583C, G584C, H587C, Q592C, G594C, P596C, and Y597C (rectification factor is switched from positive to negative, P_K/P_{Na} is increased, and $V_{0.5}$ of activation is shifted in the depolarizing direction). The remaining seven maintain the mutant behavior: W585C, L586C, N588C, L589C, G590C, D591C, and I593C. However, the enhancement of their sensitivity to MTSET by DTT treatment (Fig. 6 D) reveals that the introduced cysteine side chains at these positions indeed are reduced, despite the maintained mutant behavior (i.e., high-impact positions).

Periodicity of Mutation-induced Perturbations in Channel-gating Function

The distribution of these seven high-impact positions along the 583–597 segment gives a hint of α-helical pattern. To further explore this possibility, mutation-induced perturbations in channel activation gating (after DTT treatment) are used to analyze α-helical periodicity as described (Cornette et al., 1987; Li-Smerin et al., 2000) (see MATERIALS AND METHODS). Fig. 7 A illustrates the Fourier transform power spectrum of the 583–597 segment. For K595C that does not produce functional channels, the value <V> of this segment is used (see MATERIALS AND METHODS; Li-Smerin et al., 2000). The major peak occurs at an angular frequency of 94°, close to the expected peak of an ideal α-helix (100°). The α-helical tendency, as calculated by α-PI, is 1.64. Although the α-PI is less than two, the level considered as a strong indicator of α-helix formation, it nevertheless supports such a helical tendency. We further analyze the α-helix forming tendency along the S5-P linker from positions 571 to 613, using a 15-aa sliding window (Fig. 7 B). The analysis indicates that the middle part of this linker has the strongest likelihood of forming an α-helix. The amino end and especially the carboxyl end have little or no sign for long α-helices.

"Phenotype Switch" Induced by MTSET- or MTSES-modification of Cysteine Side Chains at the External Pore Entrance

We have shown previously that MTSET or MTSES modification of S631C in HERG induces a switch of channel phenotype from WT-like to mutant (disrupting C-type inactivation and K^+ selectivity) (Fan et al., 1999). These are similar to the mutant phenotype created by replacing S631 with a positively charged or a negatively charged residue (S631K and S631E, respectively) (Fan et al., 1999). In one-dimensional sequence, 631 is at the carboxyl end of the P-loop (Fig. 1). In three-dimensional space, position 631 is situated at the external entrance to the pore (Doyle et al., 1998). If the HERG

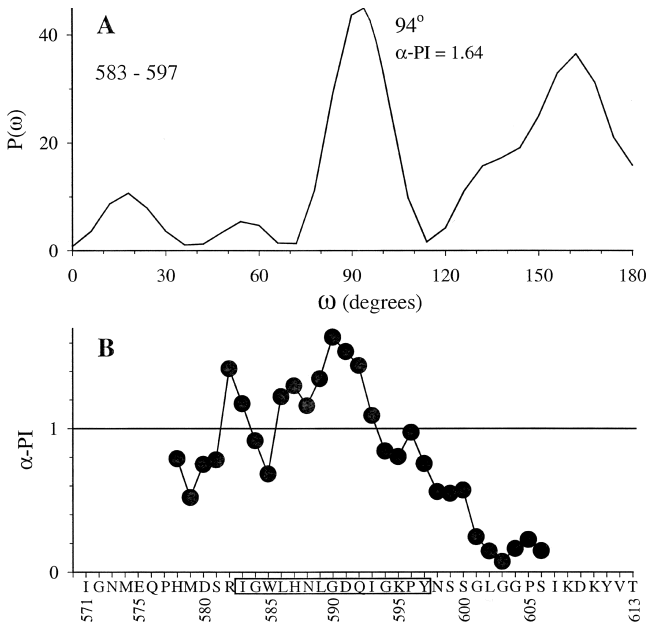

FIGURE 7. Analysis of α-helical periodicity in the S5-P linker based on perturbations of activation gating induced by cysteine mutations (data from DTT-treated channels). The methods of calculating the Fourier transform power spectrum (P(ω) vs. ω) and α-periodicity index (α-PI) are described in MATERIALS AND METHODS. (A) Fourier transform power spectrum of $|\Delta\Delta G_o|$ values for the segment of 583–597 (value for the nonfunctional K595C is taken from <V>). (B) Windowed α-periodicity index analysis of S5-P linker of HERG. The α-PI values are calculated with a 15-residue sliding window and plotted against WT residues with selected position numbers along the abscissa (putative α-helix "583–597" is boxed).

outer mouth has a narrow dimension here, side chains at position 631 from all four subunits can be very close to each other. Adding multiple charges here (in a homotetramer of S631K or S631E, or after simultaneous modification of several S631C side chains by MTSET or MTSES) will lead to an electrical repulsion between like charges. These repulsive forces between 631 side chains around the external pore entrance may interfere with conformational changes necessary for an efficient C-type inactivation and a proper K^+ selectivity.

T613 is at the amino end of the P-loop in one-dimensional sequence (Fig. 1). If it is also close to the external entrance of the pore, we predict that MTSET or MTSES modification of T613C should induce a phenotype switch, similar to the effects of MTS modification on S631C. Fig. 8 B shows tail I-V relationships of T613C before and after MTSET or MTSES modification. Before MTS treatment, the tail I-V relationships manifest a prominent negative slope in the V_r range of 30 to −60 mV (strong C-type inactivation) and an E_{rev} close to −100 mV (high P_K/P_{Na}). After modification by either MTSET or MTSES, the tail I-V relationships have a positive slope in the same V_r range (C-type inactivation disrupted) and the E_{rev} values are shifted toward 0 mV

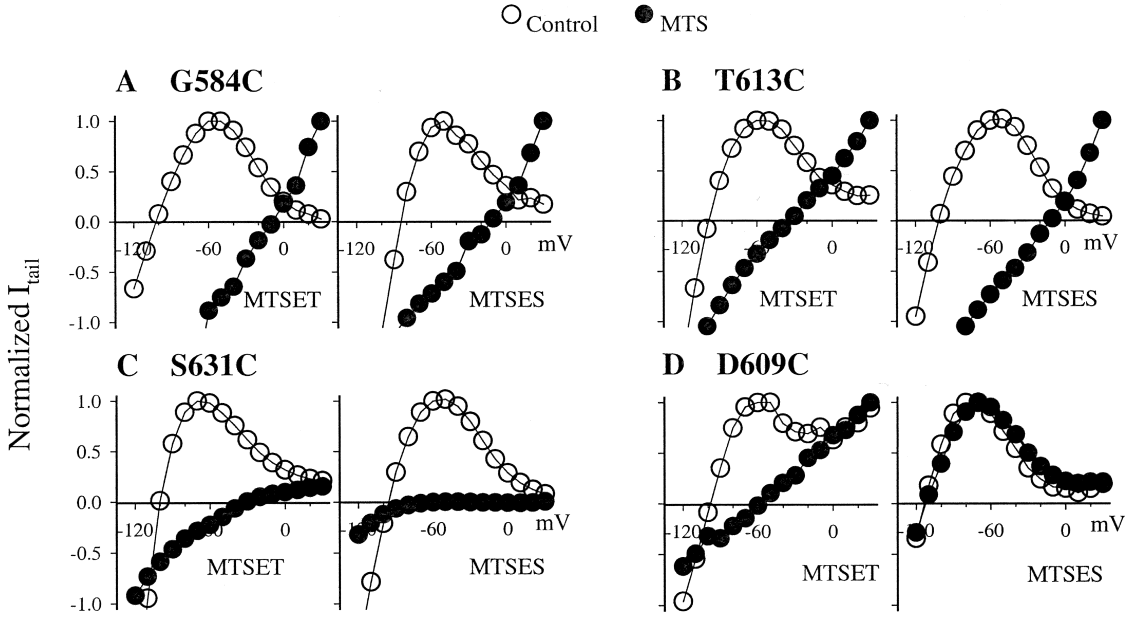

FIGURE 8. Effects of MTSET and MTSES on the I-V relationship and E_{rev} of four cysteine mutants: G584C (A), T613C (B), S631C (C), and D609C (D). In all cases oocytes have been DTT treated. The recording conditions, voltage clamp protocol, and data analysis are the same as those described for Fig. 2. After control data (open circles) are obtained, the cells are exposed to MTSET (1 mM) or MTSES (1 mM) while the channels are activated by constant pulses from V_h −80 to 20 mV for 1 s once per 30 or 60 s till changes in currents reach a steady state. The MTS reagents are washed out for ≥10 min and then currents after MTS modification (closed circles) are recorded.

(P_K/P_{Na} reduced). These results confirm our prediction.

Among the other eight positions in the outer vestibule region where cysteine substitution sustains the WT-like behavior and MTS modification has a marked impact on channel function (Fig. 6), only one has the same response as those of S631C and T613C. Fig. 8 A shows that MTSET or MTSES modification of G584C also induces a phenotype switch. This position is 30 amino acids away from the pore entrance in the one-dimensional sequence (Fig. 1). However, the similarity in the MTS effects between G584C and the two pore-entrance residues suggests that in three-dimensional space G584 may be also close to the pore entrance.

Fig. 8 C shows that MTSET and especially MTSES cause a marked suppression of S631C channel conductance. This is not seen in either T613C (Fig. 8 B) or G584C (Fig. 8 A). These observations suggest that 631 side chains may be deeper into the pore than those of 613 or 584. Therefore, in addition to the charge effect on conformational changes around the pore entrance, MTS modification also causes a steric hindrance to current flow through the S631C pore.

Although MTSET modification of D609C also induces a phenotype switch, similar to the effects of MTSET on the pore-entrance residues, MTSES has little effect on D609C (Fig. 8 D). Therefore, the MTSET effects on D609C are due to a mechanism different from an induced electrical repulsion between like charges.

DISCUSSION

We perform cysteine-scanning mutagenesis on 51 residues that line the outer vestibule of the HERG channel (positions 571–613 of the S5-P linker and positions 631–638 of the P-S6 linker). Three of the cysteine-substituted channels do not produce functional expression. Of the other 48, we study the effects of cysteine substitution on channel function before and after DTT treatment and the effects of MTS modification. Fig. 9 A summarizes the major findings reported in this study, including: (a) disulfide-forming capability of introduced cysteine side chains, (b) channel phenotypes when the introduced cysteine side chains are in the reduced (free thiol) or oxidized (disulfide bonded) state, (c) effects of MTSET modification, and (d) impact of modifying side chain properties on the HERG channel function deduced from the above data. Disulfide bond formation before DTT or disulfide reduction by DTT is probably not an "all-or-none" reaction. However, from the pronounced changes in channel behavior and/or from the marked increase in MTSET sensitivity after DTT treatment, we can make clear-cut conclusions as to whether disulfide bond formation or reduction has occurred or not. Based on the results, we divide the degrees of impact of side chain modification into three groups: high-impact (cysteine substitution destroys functional expression, or disrupts channel function even when the thiol groups are in the reduced state); intermediate-impact (cysteine substitution in the free thiol

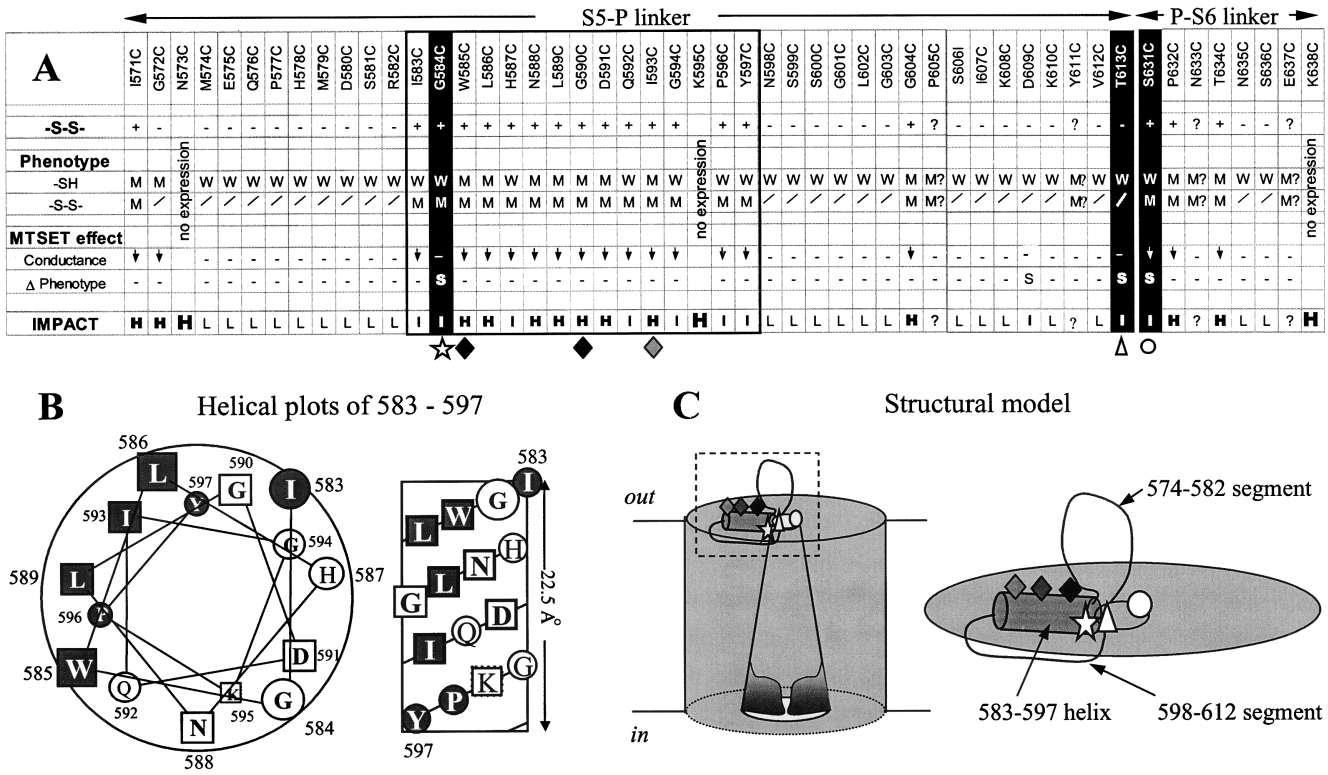

FIGURE 9. (A) Summary table of effects of cysteine substitutions in the S5-P and P-S6 linkers on HERG channel function and response to MTSET. -S-S-, cysteine thiol side chains capable of forming disulfide bonds (+), or not (−). ?, data not conclusive. Phenotype, WT-like (W, strong C-type inactivation and high K^+ selectivity) or mutant (M, disrupted C-type inactivation and low K^+ selectivity), evaluated when thiol side chains are in reduced state (−SH) or in disulfide bonded state (-S-S-). M?, cysteine mutants have mutant behavior but the status of cysteine side chains unclear. /, not applicable because the introduced thiol side chains cannot form disulfide bonds. MTSET effect, decrease in channel conductance (downward arrow) or a switch of channel phenotype from WT-like to mutant (S). –, no effect. The 583–597 segment is boxed. G584C, W585C, G590C, I593C, T613C, and S631C are highlighted by different symbols below the table. (B) Plots of α-helical wheel (left) and α-helical net (right) of the 583–597 segment. Position numbers are labeled. Hydrophobic side chains are shaded gray. Hydrophilic side chains and glycine have no shade. Squares denote high-impact positions, while circles denote intermediate-impact positions. (C) Proposed structural model of HERG's pore domain. (Left) The helix formed by residues 583–597 is represented by a short cylinder. Symbols correspond to those in A and represent G584, W585, G590, I593, T613, and S631. For clarity, only one each of 583–597 helix, T613 and S631 are drawn for the channel. The HERG channel pore is drawn as a right side up "teepee" to reflect the following points: (1) The outer mouth of HERG may be narrower than that of Shaker or KcsA due to (a) a lack of important hydrogen bonds that can stabilize the outer mouth in the open state, and (b) the insertion of extra sequences from the S5-P linkers. (2) The inner mouth of HERG may be wider than that of Shaker or KcsA because it can accommodate drug molecules of large sizes (Mitcheson et al., 2000). (Right) An enlarged view of the boxed area. The model has the 583–597 helix orientated parallel to the plane of the cell membrane, with its NH_2 end situated close to the pore entrance, so that G584 (star), like the two positions at the two ends of the P-loop, T613 (triangle) and S631 (circle), sits at the edge of extracellular pore entrance, with residues W585, G590, and I593 (diamonds) capable of interacting with a bound scorpion peptide toxin, ErgTx (Pardo-Lopez et al., 2002). The 574–582 segment forms an extracellular loop of low-impact positions. The 598–612 segment returns from the carboxyl end of the 583–597 helix to the pore, and along the way makes contacts with the outer surface of the channel at high- and intermediate-impact positions (604 and 609, respectively).

state is well tolerated, but further MTSET modification produces a significant impact on channel function); and low-impact (neither cysteine substitution nor further MTSET modification impacts on channel function).

Unique Structure of HERG's Outer Vestibule: Role of 583–597 Helix

We proposed previously that there are fundamental differences between HERG and Shaker in the outer vestibule structure and the molecular motions underlying their C-type inactivation processes (Dun et al., 1999a; Fan et al., 1999; Tseng, 2001). Our proposal was based on the following observations: (a) In the Shaker channel, side chains at position 449 (equivalent of 631 in HERG, Fig. 1) interact directly with TEA bound to the outer mouth (Heginbotham and MacKinnon, 1992), whereas in HERG, side chains at 631 are shielded from the electrostatic effects of bound TEA (Pardo-Lopez et al., 2002). (b) T449E and T449K facilitate C-type inactivation in the Shaker (Lopez-Barneo et al., 1993), whereas S631E and S631K disrupt C-type inactivation

in HERG (Fan et al., 1999). (c) MTS modification of T449C is strongly facilitated by C-type inactivation (Liu et al., 1996), whereas MTS modification of S631C has no state dependence (Dun et al., 1999b). (d) C-type inactivation in Shaker is associated with a decrease in P_K/P_{Na} (Starkus et al., 1997), whereas in HERG a disruption of C-type inactivation is associated with a decrease in P_K/P_{Na} (this report). (e) Two scorpion peptide toxins, charybdotoxin (ChTx) and BeKm-1, share a general three-dimensional structure (Miller, 1995; unpublished data), but use different interaction surfaces and different mechanisms in suppressing their respective target channels, Shaker and HERG (Hidalgo and MacKinnon,1995; unpublished data). The differences between ChTx and BeKm-1 most likely reflect differences in the conformation of the receptor site: the outer vestibule of target channel.

The most striking finding in our study is the critical role in the HERG channel function played by the 583–597 segment in the middle of the S5-P linker. We propose a structural model (Fig. 9 C) in which the 583–597 segment forms an α-helix (583–597 helix), with its amino end sitting at the pore entrance and the whole helix exposed to the extracellular aqueous environment. This is based on the following observations: (a) analysis of side chain properties suggests that this segment can form an amphipathic α-helix (Fig. 9 B), and α-helix periodicity analysis of mutation-induced perturbations of channel function supports such a secondary structure (Fig. 7), (b) MTS modification of G584C induces a phenotype-switch similar to that seen with MTS modification of two pore-entrance residues (T613C and S631C), whereas none of the other cysteine mutants have such a response, (c) all residues in the 583–597 segment are accessible to extracellular MTS reagents (Fig. 6 D), and (d) several resides along this segment (W585, G590, Q592 and I593) are critical for the binding of extracellular peptide toxins, ErgTx (Pardo-Lopez et al., 2002) and BeKm-1 (unpublished data). Such an α-helix will be ~22 Å in length (Fig. 9 B). When oriented parallel to the plane of the cell membrane with its amino end near the pore entrance (Fig. 9 C), its carboxyl end will be able to reach the voltage-sensing domain. This is based on: (a) the dimension of KcsA (Doyle et al., 1998), and (b) a study using "molecular tapes" to estimate the distance between the pore entrance and the voltage-sensing domain of the Shaker channel (Blaustein et al., 2000). In this way, this 583–597 helix can serve as a bridge of communication between the outer mouth and the voltage-sensing domain. We hypothesize that depolarization-induced motions in the S4 domain (outward and/or rotational movements along with a change in the S4 tilt [Cha et al., 1999, Glauner et al., 1999]) can change the orientation of this 583–597 helix or push it toward the pore. This then pinches off the external entrance and causes C-type inactivation. Upon membrane repolarization, a reversal of the above S4 movements then relieves the force on the 583–597 helix, allowing the pore to reopen (recovery from C-type inactivation). These tightly choreographed molecular motions can account for the high voltage-sensitivity and the rapid onset and recovery kinetics of C-type inactivation in the HERG channel.

In Fig. 9 C, the 583–597 helix is depicted as being oriented parallel to the plane of the cell membrane. However, its orientation and interactions with other domains of the channel may change during channel gating (H. Robert Guy, personal communication). It is possible that in some gating state, part of the 583–597 helix may become more parallel to the pore axis, with its amino terminus participating in pore lining. This can explain the differential effects of MTS modification of thiol groups introduced to three consecutive positions at the amino terminus of this segment: 583–585. As discussed above, the phenotype-switch induced by either MTSET or MTSES modification of G584C can be explained by proposing that residues 584 lie at the pore entrance, with their introduced thiol side chains pointing toward the pore axis. If this part of the helix becomes somewhat parallel to the pore axis, 583 will be deeper into the pore and 585 will be on the channel surface. Increasing 583C side chain volume by either MTSET or MTSES will cause a steric hindrance to current flow through the pore. This can explain why I583C channel conductance is markedly reduced by either MTS reagent (Figs. 3 B and 4 B). On the other hand, adding positive charges to the 585 thiol side chains by MTSET will cause a positive shift in the local surface potential and reduce $[K^+]$ around the pore, leading to a decrease in channel conductance. MTSES should have the opposite effects. This may explain why W585C channel conductance is decreased by MTSET but increased by MTSES (Figs. 3 C and 4 C).

Implications of Other High- and Intermediate-impact Positions in the Structure-function Relationship of HERG

High-impact positions at the outer end of S5 and in the P-S6 linker. The crystal structure of a K channel pore domain, KcsA, shows that the outer end of M1 (S5 equivalent) and P-M2 linker (P-S6 equivalent) are close to each other in three-dimensional space (Doyle et al., 1998). Functional studies on the Shaker channel further suggest that the outer end of S5 (E418) interacts with the P-S6 linker (V451/G452) (Fig. 1) (Gandhi et al., 2000; Larsson and Elinder, 2000; Ortega-Saenz et al., 2000). We identify one group of high-impact positions at the outer end of S5 (571–573) and another group in the P-S6 linker (632–634). It is possible that in the HERG channel, region "571–573" interacts with re-

gion "632–634" through their side chains and peptide backbones during channel gating, and these interactions are important for channel function. Further experimentation is needed to confirm these interactions (e.g., by double cysteine substitution and testing for inter- or intrasubunit disulfide formation involving the introduced thiol groups), and to determine their role in channel function.

Effects of MTS modification of D609C is charge-specific. A string of three charges, two lysines flanking an aspartate (KDK), is located close to the amino end of the P-loop (positions 608–610, Fig. 1). Are these charges important for channel function? For example, can they contribute to the voltage-sensitivity of C-type inactivation in the HERG channel? Do they dominate the surface potential around the pore, so that they can influence the pore conductance via effects on the local K^+ concentration? Neutralizing any one of these charges (K608C, D609C, or K610C) does not perturb channel function (intact C-type inactivation and strong K^+ selectivity). Modification of K608C or K610C by MTSET, and more importantly by MTSES, has little impact on channel function or pore conductance. Fig. 8 D shows that although MTSES has little effect on D609C, MTSET modification induces a phenotype switch: C-type inactivation and K^+ selectivity are disrupted. It is possible that the repulsive forces between the positive charge attached to the thiol side chain at 609 by MTSET and the positive charges on the two flanking lysine side chains can limit the backbone flexibility or perturb the conformation to such an extent that the pore function is disrupted. These observations rule out any major role played by these three charged residues in influencing either the voltage-sensitivity of C-type inactivation, or the local surface potential around the pore.

HERG has a "Floppy" Outer Mouth

Conformational flexibility of the outer mouth in the HERG channel is key to its function. In this regard, the reduced hydrogen bonding capability around the outer mouth of the HERG channel, as suggested by the amino acid sequence alignment shown in Fig. 1, is an important contributing factor. In the Shaker channel, oxygen of the carboxylate side chain of E418 can form a hydrogen bond with the peptide backbone nitrogen in the P-S6 linker (451/452) (Larsson and Elinder, 2000; Ortega-Saenz et al., 2000). The E418 equivalent in the HERG channel, I571, does not have the oxygen donor for hydrogen bonding. In the Shaker, the nitrogen of W434 forms a hydrogen bond with the hydoxyl side chain of Y445 (Doyle et al., 1998). Again, in HERG the equivalent residues (Y616 and F627) cannot form a hydrogen bond.

In our structural model for HERG's outer mouth, this flexibility allows the 583–597 helix to assume different orientations and may become intercalated into the pore lining in some gating state. Therefore, rigidifying the outer vestibule structure by disulfide bond formation involving cysteine side chains introduced here is detrimental to C-type inactivation and K^+ selectivity. Cysteine substitutions of critical residues at high-impact positions, or MTS modifications of pore-entrance residues, may also reduce the conformational flexibility and thus produce the same mutant phenotype. In the HERG mutants examined here, a disruption of pore properties (loss of C-type inactivation and K^+ selectivity) goes hand-in-hand with a hyperpolarizing shift in the voltage dependence of activation (Fig. 6, A–C). This strong association suggests that rigidifying the outer mouth structure makes conformational changes induced by S4 movements propagate to the outer mouth region more efficiently, thus making the HERG channel open more readily. Therefore, we propose that a "floppy" outer mouth in the WT HERG channel makes it more reluctant to open but easier to close (C-type inactivate) than the Shaker channel.

The authors would like to thank Dr. H. Robert Guy (National Cancer Institute, National Institutes of Health) for helpful discussion.

This study is supported by HL 46451 from the National Heart, Lung, and Blood Institute; National Institutes of Health; and a Grant-in-Aid Award from the American Heart Association/Mid-Atlantic Affiliate (G.N. Tseng).

Submitted: 30 July 2002
Revised: 24 September 2002
Accepted: 30 September 2002

REFERENCES

Blaustein, R.O., P.A. Cole, C. Williams, and C. Miller. 2000. Tethered blockers as molecular 'tape measures' for a voltage-gated K^+ channel. *Nat. Struct. Biol.* 7:309–311.

Cha, A., G.E. Snyder, P.R. Selvin, and F. Bezanilla. 1999. Atomic scale movement of the voltage-sensing region in a potassium channel measured via spectroscopy. *Nature.* 402:809–813.

Cornette, J.L., K.B. Cease, H. Margalit, J.L. Spouge, J.A. Berzofsky, and C. DeLisi. 1987. Hydrophobicity scales and computational techniques for detecting amphipathic structures in proteins. *J. Mol. Biol.* 195:659–685.

Doyle, D.A., J.M. Cabral, R.A. Pfuetzner, A. Kuo, J.M. Gulbis, S.L. Cohen, B.T. Chait, and R. MacKinnon. 1998. The structure of the potassium channel: molecular basis of K^+ conduction and selectivity. *Science.* 280:69–77.

Dun, W., M. Jiang, and G.-N. Tseng. 1999a. Allosteric effects of mutations in the extracellular S5-P loop on the gating and ion permeation properties of *hERG. Pflugers Arch.* 439:141–149.

Dun, W., M. Jiang, S. Zeng, and G.-N. Tseng. 1999b. Differences in the effects and state-dependence of MTS modification of an outer mouth cysteine residue reveal differences between *HERG* and *Shaker* in structural rearrangements involved in C-type inactivation. *Circulation.* 100:I842.

Fan, J.-S., M. Jiang, W. Dun, T.V. McDonald, and G.-N. Tseng. 1999. Effects of outer mouth mutations on *hERG* channel function: a comparison with similar mutations in *Shaker. Biophys. J.* 76:3128–3140.

Fedida, D., N.D. Maruoka, and S. Lin. 1999. Modulation of slow in-

activation in human cardiac Kv1.5 channels by extra- and intracellular permeant cations. *J. Physiol.* 515:315–329.

Gandhi, C.S., E. Loots, and E.Y. Isacoff. 2000. Reconstructing voltage sensor-pore interaction from a fluorescence scan of a voltage-gated K^+ channel. *Neuron.* 27:585–595.

Glauner, K.S., L.M. Mannuzzu, C.S. Gandhi, and E.Y. Isacoff. 1999. Spectroscopic mapping of voltage sensor movement in the *Shaker* potassium channel. *Nature.* 402:813–817.

Hancox, J.C., A.J. Levi, and H.J. Witchel. 1998. Time course and voltage dependence of expressed HERG current compared with native "rapid" delayed rectifier K current during the cardiac ventricular action potential. *Pflugers Arch.* 436:843–853.

Heginbotham, L., and R. MacKinnon. 1992. The aromatic binding site for tetraethylammonium ion on potassium channels. *Neuron.* 8:483–491.

Hidalgo, P., and R. MacKinnon. 1995. Revealing the architecture of a K^+ channel pore through mutant cycles with a peptide inhibitor. *Science.* 268:307–310.

Hoshi, T., W.N. Zagotta, and R.W. Aldrich. 1991. Two types of inactivation on Shaker K^+ channels: effects of alterations in the carboxy-terminal region. *Neuron.* 7:547–556.

Klemic, K.G., C.-C. Shieh, G.E. Kirsch, and S.W. Jones. 1998. Inactivation of Kv2.1 potassium channels. *Biophys. J.* 74:1779–1789.

Larsson, H.P., and F. Elinder. 2000. A conserved glutamate is important for slow inactivation in K^+ channels. *Neuron.* 27:573–583.

Li-Smerin, Y., D.H. Hackos, and K.J. Swartz. 2000. α-Helical structure elements within the voltage-sensing domains of a K^+ channel. *J. Gen. Physiol.* 115:33–49.

Liu, Y., M.E. Jurman, and G. Yellen. 1996. Dynamic rearrangement of the outer mouth of a K^+ channel during gating. *Neuron.* 16: 859–867.

Lopez-Barneo, J., T. Hoshi, S.H. Heinemann, and R.W. Aldrich. 1993. Effects of external cations and mutations in the pore region on C-type inactivation of Shaker potassium channels. *Receptors Channels.* 1:61–71.

Miller, C. 1995. The charybdotoxin family of K^+ channel-blocking peptides. *Neuron.* 15:5–10.

Mitcheson, J.S., J. Chen, and M.C. Sanguinetti. 2000. Trapping of a methanesulfonanilide by closure of the HERG potassium channel activation gate. *J. Gen. Physiol.* 115:229–239.

Ortega-Saenz, P., R. Pardal, A. Castellano, and J. Lopez-Barneo. 2000. Collapse of conductance is prevented by a glutamate residue conserved in voltage-dependent K^+ channels. *J. Gen. Physiol.* 116:181–190.

Panyi, G., Z.-F. Sheng, L.-W. Tu, and C. Deutsch. 1995. C-type inactivation of a voltage-gated K^+ channel occurs by a cooperative mechanism. *Biophys. J.* 69:896–903.

Pardo-Lopez, L., M. Zhang, J. Liu, M. Jiang, L.D. Possani, and G.-N. Tseng. 2002. Mapping the binding site of a HERG-specific peptide toxin (ErgTx) to the channel's outer vestibule. *J. Biol. Chem.* 277:16403–16411.

Rasmusson, R.L., M.J. Morales, R.C. Castellino, Y. Zhang, D.L. Campbell, and H.C. Strauss. 1995. C-type inactivation controls recovery in a fast inactivating cardiac K^+ channel (Kv1.4) expressed in *Xenopus* oocytes. *J. Physiol.* 489:709–721.

Rasmusson, R.L., M.J. Morales, S. Wang, S. Liu, D.L. Campbell, M.V. Brahmajothi, and H.C. Strauss. 1998. Inactivation of voltage-gated cardiac K^+ channels. *Circ. Res.* 82:739–750.

Sanguinetti, M.C., C. Jiang, M.E. Curran, and M.T. Keating. 1995. A mechanistic link between an inherited and an acquired cardiac arrhythmia: HERG encodes the I_{Kr} potassium channel. *Cell.* 81: 299–307.

Schreibmayer, W., H.A. Lester, and N. Dascal. 1994. Voltage clamping of *Xenopus* laevis oocytes utilizing agarose-cushion electrodes. *Pflugers Arch.* 426:453–458.

Smith, P.L., T. Baukrowitz, and G. Yellen. 1996. The inward rectification mechanism of the HERG cardiac potassium channel. *Nature.* 379:833–836.

Spector, P.S., M.E. Curran, A. Zou, M.T. Keating, and M.C. Sanguinetti. 1996. Fast inactivation causes rectification of the I_{Kr} channel. *J. Gen. Physiol.* 107:611–619.

Splawski, I., J. Shen, K.W. Timothy, M.H. Lehmann, S.G. Priori, J.L. Robinson, A.J. Moss, P.J. Schwartz, J.A. Towbin, G.M. Vincent, and M.T. Keating. 2000. Spectrum of mutations in long-QT syndrome genes *KvLQT1*, *HERG*, *SCN5A*, *KCNE1*, and *KCNE2. Circulation.* 102:1178–1185.

Starkus, J.G., L. Kuschel, M.D. Rayner, and S.H. Heinemann. 1997. Ion conduction through C-type inactivated *Shaker* channels. *J. Gen. Physiol.* 110:539–550.

Tseng-Crank, J.C.L., G.-N. Tseng, A. Schwartz, and M.A. Tanouye. 1990. Molecular cloning and functional expression of a potassium channel cDNA isolated from a rat cardiac library. *FEBS Lett.* 268:63–68.

Tseng, G.-N. 2001. I_{Kr}: the hERG channel. *J. Mol. Cell. Cardiol.* 33: 835–849.

Yellen, G., D. Sodickson, T.-Y. Chen, and M.E. Jurman. 1994. An engineered cysteine in the external mouth of a K^+ channel allows inactivation to be modulated by metal binding. *Biophys. J.* 66: 1068–1075.

Zhou, J., Q. Gong, B. Ye, Z. Fan, J.C. Makielski, G.A. Robertson, and C.T. January. 1998. Properties of HERG channels stably expressed in HEK 293 cells studied at physiological temperature. *Biophys. J.* 74:230–241.